Bragg coherent diffractive imaging of ferromagnetic nickel nanoparticles

J. W. Kim[1,2], S. Manna[3], R. Harder[2], J. Wingert[1], E. E. Fullerton[3], and O. G. Shpyrko[1]

[1]*Department of Physics, University of California-San Diego, La Jolla, California 92093-0319, USA*
[2]*Advanced Photon Source, Argonne National Laboratory, Argonne, Illinois 60439, USA*
[3]*Center for Memory and Recording Research, University of California-San Diego, La Jolla, California 92093-0401, USA*

Abstract

We synthesized Ni nanoparticles with atmospheric-thermal chemical vapor deposition method and investigated their lattice distortions and defects using Bragg coherent diffractive imaging. Because the strain can alter magnetic properties in ferromagnetic materials, it is important to study the lattice distortion and structural imperfection. As a result of Bragg coherent diffractive imaging, we found that the Ni nanocubes have a deformation-free zone in the middle. In addition, defects such as dislocation and twin domain defects were detected in other Ni nanoparticles based on the Bragg diffraction images and patterns. The imaging of nanoparticles can help better understand their growth mechanisms and improve the design and synthesis method of nanoparticles.

Introduction

Nickel nanoparticles have attracted considerable interest due to their varied ferromagnetic properties [1-2]. A wide range of applications in data storage or medical applications have driven significant research on ferromagnetic nanoparticles [3-5]. Because the ferromagnetic property can be altered by both the shape and internal strain, it is important to investigate the lattice distortion of ferromagnetic nanoparticles as well as their ferromagnetic properties [6-8]. We have synthesized single-crystal Ni nanocubes using atmospheric-thermal chemical vapor deposition (CVD) method and investigated the details of 3D displacement fields within an individual Ni nanocube and related Ni nanoparticles [9].

Bragg coherent diffractive imaging (CDI) has been used in various fields of material science due to its ability to visualize the 3D displacement field, as well as the identification of presence and locations of defects. Thus, it has been employed to explore defects dynamics in battery nanomaterials during charge/discharge process [10], dislocation propagation in nanocrystals during the growth [11], dislocation dynamics during phase transformation [12], strain induced by static pressure [13-14], strain induced by catalysis [15], strain induced by solid angle deficiency in multiple twinned nanoparticle [16], and strain induced by ion-implantation [17].

Experimental Details

In a Bragg CDI measurements, a sample, incident x-ray beam and a detector are aligned such that the Bragg peak appears on the detector in the far field. The 2D diffraction patterns on the detector are recoded while the sample is rotated by a small angular step sizes, ~0.01°, through a total angle of ~0.4°, with respect to the incident x-ray beam. In order to obtain the 3D diffraction pattern, these 2D diffraction patterns need to be stacked together after data acquisition process, which is known as a rocking scan. Using the phase retrieval algorithm applied to the 3D diffraction intensity, we can obtain the shape of the nanoparticle and the displacement field projected onto the momentum transfer vector. The amplitude and the phase result from the phase retrieval correspond to the Bragg electron density and the displacement of atoms from their equilibrium positions, respectively [18-19]. If there is a portion that doesn't satisfy the Bragg condition, it is invisible in the reconstructed image [20]. A value of 2π phase is equivalent to a displacement of a d-spacing of Bragg reflection plane. The Bragg CDI measurements were performed at Sector 34-ID-C of the Advanced Photon Source (APS) radiation synchrotron facility. An upstream monochromator was used to select E = 9.0 KeV x-rays, which were focused onto the sample using Kirkpatrick-Baez mirrors that focused the beam to a $2\mu m \times 2\mu m$ region. The resulting diffraction patterns were measured using a

charge-coupled device (CCD) with 22.5 μm pixels located along the detector arm at a distance of 0.75 m beyond the sample (for more details, please see the Data Acquisition section in the Supplementary Material). In this experiment, we reconstruct the 3D distribution of Bragg electron density and the 3D lattice displacement field projected along (111) direction with 18~30 nm spatial resolution, which is defined by the phase retrieval transfer function (for more details, please see the Phase Retrieval Transfer Function section in the Supplementary Material), depending on individual nanoparticles.

In this study, we synthesized single-crystal Ni nanocubes using in-house atmospheric-thermal chemical vapor deposition (CVD) comprising of a Lindberg blue furnace with a quartz tube installed. An Ar carrier gas is flowed through the quartz tube using an MKS thermal mass flow controller while the downstream end of the CVD setup is closed off to outside atmosphere with a bubbler. Powdered $NiCl_2 \cdot 6H_2O$ in a Ni boat is placed alongside $SiO_2||Si$ substrate within a quartz tube which inserted inside the CVD furnace at 200°C for 10 mins. After that, the temperature is increased to 650°C for another 10 mins.

Results and Discussion

Because the low-index facets (i.e. {100}, {110}, and {111}) have the smallest specific surface energies in face-centered-cubic crystals, these facets play an important role in the growth of nanoparticles [21]. The growth rates of all facets are comparable until the {100} facets stop growing [22]. The shape of the nanocube is formed by the continuing growth of the other two facets. In other words, the edges and vertices of the nanocube are completed during the later development. The study on the growth mechanism of metal nanocubes using transmission electron microscopy revealed that nanoparticles appear to be round and rotate at the early stage of growth and then become more stationary [22].

Figures 1a and 1b show a schematic of experimental setup with SEM image

and 3D diffraction intensity made up of 41 2D diffraction patterns. Figures 1c and 1d represent the Bragg electron density with phases mapped on surface with the color representing the displacement field and three horizontal slices. Most of the displacement field is green or blue, meaning that there are zero or negative displacements within the nanocube. The phase is smoothly distributed within the 3D volume of nanocube and maximum magnitude of phase is 1.05 rad, which is equivalent to the displacement 0.34Å along (111) direction. In particular, there is a spherical green zone in the middle of the nanocube, indicating that the strain is nearly free in the middle and it is relatively concentrated in vertices or edges. The spherical zone in the middle and the outer portion correspond to the rounded shape formed at early stage, and edges and vertices shaped at the later stage, respectively. As mentioned above, a metal nanocube rotates at early stage and facets are developed at the end [22]. The previous study and our observation allows us to postulate that the strain, if it is at early stage of growth, is released while rotating and accommodated at vertices and/or edges during the development of facets.

The 3D strain distribution of the nanocube, which is obtained by taking the derivative of the displacement field resulting from algorithmic phase reconstruction, the maximum magnitude of the strain is 0.05%. According to our previous study [9], this strain level is not sufficient to significantly affect the magnetic anisotropy and ground state magnetization of ferromagnetic cubes. If we have more nanocubes grown under different conditions, we can analyze the growth conditions that generate the most and least intrinsic strain and consequently the conditions that influence on the magnetic properties.

The atmospheric-CVD generated not only nanocubes, but also irregular shaped and different sized nanoparticles. Figure 2 shows a nanoparticle that has a squared horizontal cross-section and a short height, which is not as high as the nanocube. In the reconstructed images shown as Fig. 2, the overall displacement range is wider than the nanocube and there is a distinct type of displacement, of

which the angular distribution linearly varies with theta. In addition, the Bragg electron density is low at this location. This combination of low electron density and the phase vortex is indicative of a dislocation, and is in good agreement with previous studies with transmission electron microscopy, Bragg CDI and Bragg ptychography [23-25]. The defective particle may take longer time than defect-free one to grow [11]. For crystalline metal nanoparticles, dislocation inside the particles can alter the mechanical behavior of nanoparticles and consequently, may lead to distinct ferromagnetic properties. We observed that both defect-free nanocubes and defective nanoparticles were generated in the same batch consistent with previous observations of variations in geometries, sizes and strains have been observed in CVD-grown metal nanocrystals [16, 26]. The local environmental variations may lead to the different growth conditions. This is supported by the comparison of two nanoparticles having similar shape and size. Figures 3a-c show the isosurface of the amplitude, three cross-sections of amplitude and phase near the top surface, and 3D dislocations in the nanoparticle, respectively. The phase vortex in Fig. 3b is a signature of the dislocation. The core of dislocation is identified based on minimum differentials in a local neighborhood [27]. In contrast, another nanoparticle has relatively narrow range of phase distribution and no dislocations in the entire particle, shown in Figs. 3d-f.

Figure 4 shows the Bragg diffraction patterns and reconstruction results of two different Ni nanoparticles. Figs. 4a and 4f show the 3D Bragg diffraction patterns and Figs. 4b and 4g show the plots of the intensities, which are integrated in the planes perpendicular to q_1 axis. In general, the Bragg peak has the highest intensity and the intensity drops as a modulation goes far from the Bragg peak as shown in Fig. 1b. The twin domain defects in nanoparticles lead to modulations in the diffraction intensity akin to the double slit experiment. The split of the Bragg peak implies that the nanoparticles contain twin domain defects [20, 28]. This has been studied through theory and experiments [29]. In addition, as a result of phase

retrieval (for more details, please see the Phase Retrieval section in the Supplementary Material), we obtained the Bragg electron density with void regions and phase offsets between nanoparticle pieces as shown in Fig. 4. These represent that both Ni nanoparticles have twin boundary defects located in void regions between pieces of nanoparticles. The gaps between two separated pieces are approximately 60 nm and 120 nm, respectively.

A twin boundary is a special type of boundary in a face-centered cubic nanostructure, in which the atomic arrangement on one side is the mirror reflection of the arrangement of the other side. The face centered cubic crystal is made up of layers and the atoms are arranged in the stacking sequence ABC. But if there is a twin domain that shares one of these layers C, the packing sequence would be CBA, which is the reflected sequence of the original one. Figures 4d and 4i show the central cross-sections of the phase inside the defective nanocrystals taken parallel to the substrate and reveal that the disconnected piece is phase offset from the parent crystal. The phase difference between two disconnected pieces are 2.06 rad. and 0.85 rad., respectively. Because the phase offset corresponds to the width of twin defects, the deviation from the phase offset can be interpreted as roughness at the interfaces [20]. The phase change caused by twin domain defects increases by $2\pi/3$ rad. incrementally (i.e. $2\pi/3 \cdot n$ where n an integer) [20]. The phase difference 2.06 rad of a nanoparticle is close to 2.09 rad ($2\pi/3 \cdot n=1$), whereas the phase difference of the other nanoparticle 0.85 rad. has a big gap from 0 rad. ($2\pi/3 \cdot n=0$) (for more details, please see the Supplementary Material). Therefore, we conclude that both Ni nanoparticles possess twin domain defects based on the Bragg diffraction patterns and the reconstructed images. One has smooth surface roughness, whereas the other nanoparticle has rough interfaces with twin domain defect.

Conclusions

In summary, we have investigated the internal structure and displacement fields of an individual Ni nanoparticles created by an atmospheric-thermal CVD method. In a Ni nanocube, we confirmed that a spherical middle zone remained deformation-free and the displacements are distributed mostly at facets and edges. We conclude that the strain, if it is in the middle, is released and accommodated at the facets or edges during the growth process. In addition, we observed other defective Ni nanoparticles. Bragg CDI enables us to identify the buried defects and twin domain defects. In future studies, the investigation on the lattice distortions of multiple Ni nanocubes with more statistics will help better understanding of growth mechanism.

Acknowledgement

The coherent x-ray imaging work at UCSD was supported by US Department of Energy, Office of Science, Office of Basic Energy Sciences, under Contract DE-SC0001805. Crystal growth was supported by NSF Award DMR-0906957 and DMR-1411335. Use of the Advanced Photon Source, an Office of Science User Facility operated for the U.S. Department of Energy (DOE) Office of Science by Argonne National Laboratory, was supported by the U.S. D.O.E. under Contract No. DE-AC02-06CH11357.

References

[1] R. L. White, R. M. Newt and R. F. W. Pease, Magnetics, IEEE Transactions on, 33, 990–995 (1997)
[2] C. Chappert, A. Fert and F. N. Van Dau, Nat. Mater., 6, 813–823 (2007)
[3] B. Terris and T. Thomson, Journal of physics D: Applied physics, 38, R199 (2005)
[4] A. Ethirajan, U. Wiedwald, H.-G. Boyen, B. Kern, L. Han, A. Klimmer, F. Weigl, G. Kaestle, P. Ziemann, K. Fauth et al., Advanced Materials, 19, 406–410 (2007)
[5] K.M. Krishnan, IEEE transactions on magnetics 46, 2523-2558 (2010)
[6] Zhang, A. M, Cheng, S. L, Lin, J. G, and Wu, X. S. J. Appl. Phys. 117, 17B325 (2015)
[7] C. K. Xie, J. I. Budnick, W. A. Hines, B. O. Wells, and J. C. Woicik, Appl. Phys. Lett. 93, 182507 (2008)
[8] M. V. Kharlamovaa and A. Arulraj, JETP Lett. 89, 301 (2009)
[9] S. Manna, J.W. Kim, M. Lubarda, J. Wingert, R. Harder, F. Spada, F, V. Lomakin, O.G. Shpyrko, and E.E. Fullerton, AIP Advances 7, 125025 (2017)
[10] A. Ulvestad, A. Singer, J. Clark, H.-M. Cho, J. W. Kim, R. Harder, J. Maser, Y. Meng, and O. Shpyrko, Science 348, 1344–7 (2015)
[11] J. Clark, J. Ihli, A. Schenk, Y. Kim, A. Kulak, J. Campbell, G. Nisbet, F. Meldrum, and I. Robinson, Nat. Mater. 14, 780–4 (2015)

[12] A. Ulvestad, M. J. Welland, W. Cha, Y. Liu, J. W. Kim, R. Harder, E. Maxey, J.N. Clark, M. J. Highland, H. You, P. Zapol, S. O. Hruszkewycz, and G. B. Stephenson, Nat. Mater. 16, 565 (2017)
[13] W. Yang, X. Huang, R. Harder, J. Clark, I. Robinson and H. Mao, Nat. Commun., 4, 1680 (2013)
[14] X. Huang, W. Yang, R. Harder, Y. Sun, M. Lu, Y.S. Chu, I. Robinson, and H. Mao, Nano Lett. 15(11) 7644–9 (2015)
[15] A. Ulvestad, K. Sasikumar, J. W. Kim, R. Harder, E. Maxey, J. Clark, B. Narayanan, S. A. Deshmukh, N. Ferrier, P. Mulvaney, S. K. R. S. Sankaranarayanan, O. G. Shpyrko, J. Phys. Chem. Lett. 7 (15), 3008–3013 (2016)
[16] J.W. Kim, A. Ulvestad, S. Manna, R. Harder, E. Fullerton and O. G. Shpyrko, Nanoscale, 9 (35) 13153 (2017)
[17] F. Hofmann, E. Tarleton, R. Harder, N. Phillips, P. Ma, J. Clark, I. Robinson, B. Abbey, W. Liu and C. Beck, Sci. Rep. 7, 45993 (2017)
[18] I. Robinson and R. Harder, Nat. Mater., 8 (4), 291−298 (2009)
[19] M. A. Pfeifer, G. J. Williams, I. A. Vartanyants, R. Harder, and I. K. Robinson, Nature, 442 (7098), 63−66 (2006)
[20] A. Ulvestad, J. Clark, R. Harder, I. K. Robinson, and O. G. Shpyrko, Nano Lett., 15 (6), 4066−4070 (2015)
[21] Z. L. Wang, J. Phys. Chem. B, 104, 1153 (2000)
[22] H.G. Liao, D. Zherebetskyy, H. Xin, C. Czarnik, R. Ercius, H. Elmlund, M. Pan, L. W. Wang, H. Zheng, Science, 345(6199) 916-9 (2014)
[23] M. J. Hytch, J-L. Putaux, J-M. Penisson, Nature. 423, 270–273 (2003)
[24] Y. Takahashi, A. Suzuki, S. Furutaku, K. Yamauchi, Y. Kohmura, T. Ishikawa, Phys. Rev. B, 87, 121201 (2013)
[25] Y. Takahashi, Y. Inui, M. Chihara, T. Asano, R. Terawaki, and S. Noda, Phys. Rev. B. 88, 235126 (2013)
[26] J.W. Kim, S. Manna, S.H. Dietze, A. Ulvestad, R. Harder, E. Fohtung, E. E. Fullerton and O. G. Shpyrko. Appl. Phys. Lett. 105(17) 173108 (2014)
[27] A. Ulvestad, M. Menickelly, and S.M. Wild, AIP Advances 8, 015114 (2018)
[28] V. Favre-Nicolin, F. Mastropietro, J. Eymery, D. Camacho, Y. M. Niquet, B. M. Borg, M. E. Messing, L.-E. Wernersson, R. E. Algra, E. P A M. Bakkers, T. H. Metzger, R. Harder, and I. K. Robinson, New J. Phys., 12(3) 035013 (2010)
[29] M. A. G. Aranda, F. Berenguer, R. J. Bean, X. Shi, G. Xiong, S. P. Collins, C. Nave, and I.K. Robinson, J. Synchrotron Radiat., 17, 751-760 (2010)

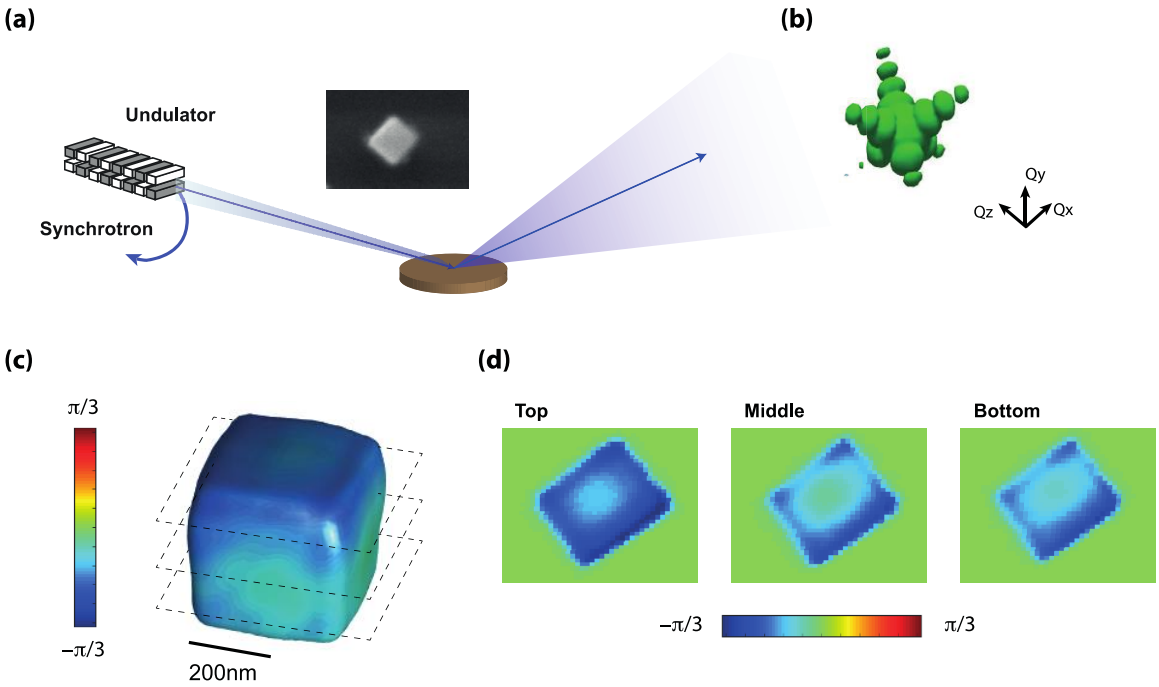

Figure 1: (a) Schematic of experimental setup with SEM image of Nickel nanocube. (b) 3D isosurface of the diffraction intensity. (c) 3D rendering of reconstructed Ni nanocube in which the color represents the phase. (d) Three cross-sections of reconstructed nanocube parallel to the substrate.

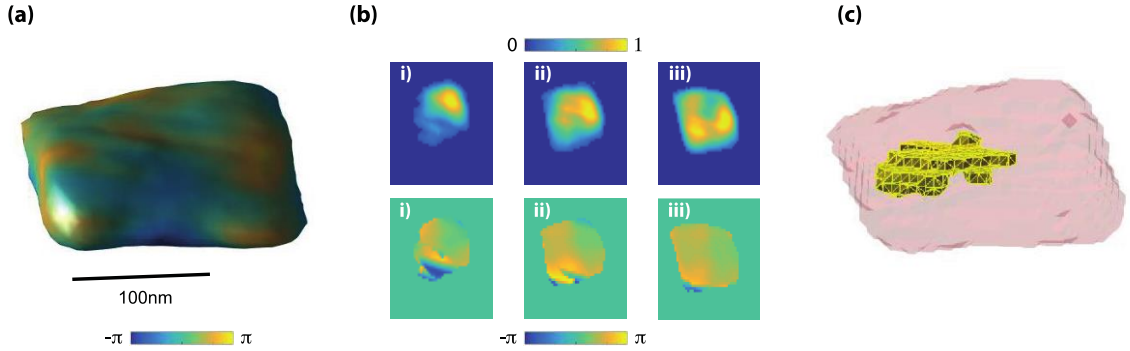

Figure 2: (a) The nanoparticle shape and the atomic displacement projected onto the surface. (b) The cross-sections of the amplitude and the phase near the top surface. The signature of the dislocations is seen in the phase. (c) The three-dimensional dislocations in the semi-transparent nanoparticle.

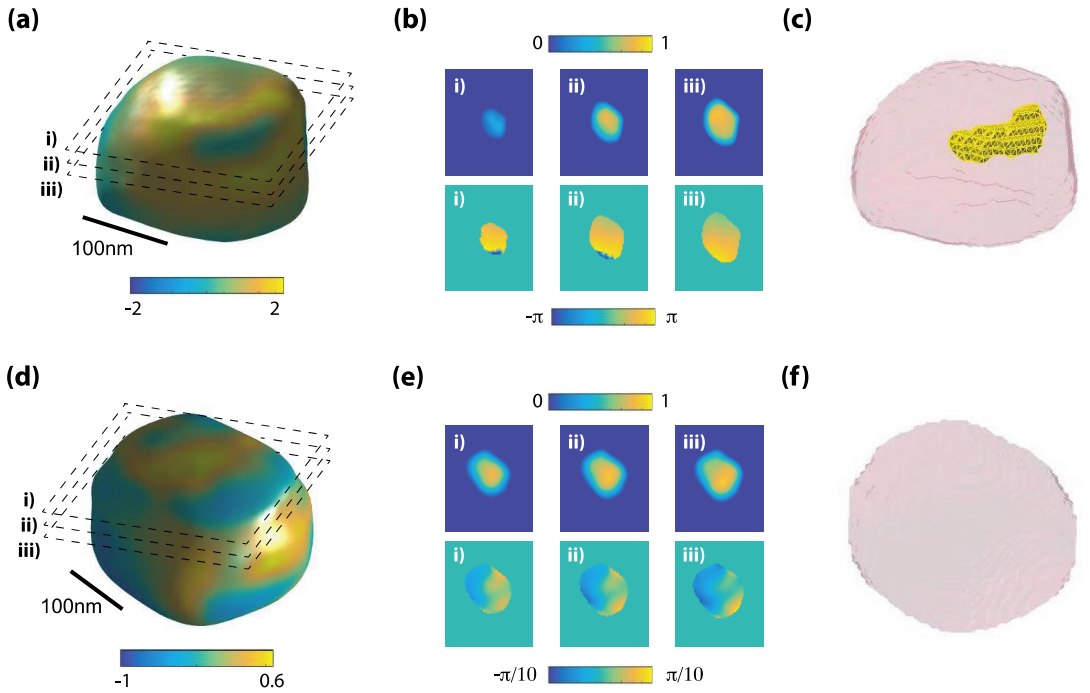

Figure 3: (a) The 3D isosurface of the amplitude and the phase mapped on the surface. (b) Three slices of the amplitude and the phase, corresponding to the dashed lines in (a). There is a signature of the dislocation in the phase. (c) The 3D dislocations located near the corner at the top. (d) The 3D isosurface of the amplitude and the phase on the surface for another nanoparticle. (e) Three slices of the amplitude and the phase near the top surface. (f) None of the dislocations is seen in the nanoparticle.

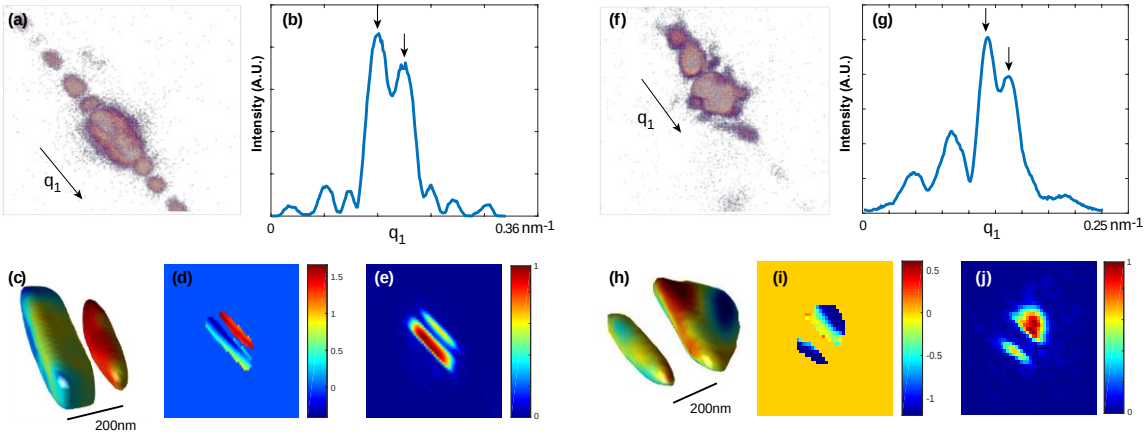

Figure 4: (a & b) The 3D diffraction intensity and integrated intensity profile along q_1 direction, respectively. Two black arrows indicate the split of the Bragg peak. (c) The 3D reconstructed image of Bragg electron density with phases mapped on the surfaces. (d & e) The phase and amplitude slices taken at the middle of reconstructed image parallel to the substrate, respectively. (f~j) The details of another Ni nanoparticle and each image corresponds to (a~e), respectively.